ACS OMEGA

http://pubs.acs.org/journal/acsodf

Article

Prediction and Verification of Performance and Emission Characteristics of Diesel/Natural Gas Dual-Fuel Engine Based on Intelligent Algorithm

Jialong Li, Taoming Wan, Haozhong Huang,* Guixin Chen, Jianguo Liang, and Baijun Lei

Cite This: *ACS Omega* 2023, 8, 18212−18224

Read Online

ACCESS | Metrics & More | Article Recommendations

ABSTRACT: With the development of computer application technologies, intelligent algorithm has been widely used in various fields. In this study, a coupled Gaussian process regression and feedback neural network (GPR-FNN) algorithm is proposed, and it is used to predict the performance and emission characteristics of a six-cylinder heavy-duty diesel/natural gas (NG) dual-fuel engine. Using the engine speed, torque, NG substitution rate, diesel injection pressure, and injection timing as inputs, an GPR-FNN model is established to predict the crank angle corresponding to 50% heat release, brake-specific fuel consumption, brake thermal efficiency, and carbon monoxide, carbon dioxide, total unburned hydrocarbon, nitrogen oxides, and soot emissions. Subsequently, its performance is evaluated using experimental results. The results show that the regression correlation coefficients of all output parameters are greater than 0.99, and the mean absolute percentage error is less than 5.9%. In addition, a contour plot is used to compare the experimental results with the GPR-FNN prediction data in detail, and the results show that the prediction model has high accuracy. The results of this study can provide new ideas for the research on diesel/natural gas dual-fuel engines.

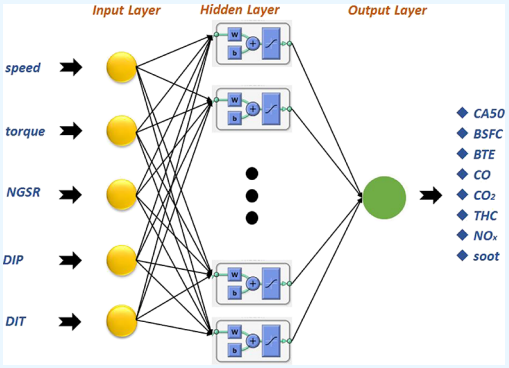

1. INTRODUCTION

With the rapid development of human society, a large amount of nonrenewable fossil fuels are consumed every year,[1,2] producing greenhouse gases that cause frequent occurrence of natural disasters,[3,4] such as global warming, melting glaciers, sea-level rise, and fires, and cause serious damage to the ecological balance. Therefore, to reduce greenhouse gas emissions, countries around the world signed the Paris Agreement, and the Chinese government proposed carbon peaking goals.[5] Internal combustion engines play an important role in many fields to aid in accelerating the human societal development.[6] However, the combustion process of internal combustion engines releases a variety of harmful gases, such as hydrocarbons, nitrogen oxides (NO_x),[7] particulate matter,[8] carbon monoxide CO, and carbon dioxide (CO_2).Therefore, choosing renewable fuels or low-carbon fuels, such as methanol[9,10] and ethanol,[11,12] can reduce fuel consumption while achieving clean combustion. Liu et al.'s[10] and Cui et al.'s[13] research studies found that adding highly reactive fuels to methanol can enhance ignition and further optimize combustion performance.

It was found that natural gas (NG), as an alternative fuel for engines,[14,15] can effectively reduce greenhouse gas emissions compared to traditional fossil fuels such as diesel, gasoline, and coal. NG has the advantages of a high hydrogen-to-carbon ratio, high octane number, abundant resources, and low price. In recent years, compression-ignition NG engines have attracted many researchers[16,17] because of their advantages such as high compression ratios.[18,19]

The automotive industry and researchers have been conducting various engine tests to improve the engine performance and reduce emissions without modifying the existing engines.[20,21] However, expensive and time-consuming experimental methods have prompted artificial intelligence to become a widely accepted option for solving difficult problems.[22,23] Common advanced machine learning methods include FNN and GPR and so on.[24] Because FNN and GPR have strong robustness, fault tolerance, and can fully approximate any complex nonlinear relationship, many researchers use them to predict the performance and emission characteristics of engines. Cui et al.[25] established the ignition delay prediction model of three-component toluene using neural networks and used genetic algorithm and particle swarm optimization algorithm to optimize the trained network. The

Received: March 10, 2023
Accepted: April 27, 2023
Published: May 11, 2023

results showed that the model can accurately predict the ignition delay time, and the correlation coefficient was higher than 0.9996. Fu et al.[26] used an FNN to forecast the engine performance and emissions of a spark-ignition engine. Taghavi et al.[27] used an FNN−genetic algorithm method to predict the combustion start point of a homogeneous charge compression−ignition engine and obtained a good result, which showed that the prediction accuracy was 0.96166. Alruqi et al.[28] used GP to model the compression−combustion engine fueled by algae biodiesel−diesel−ether and optimized the performance and emissions of the engine using Bayesian algorithm. The results showed that adding ether can improve the braking thermal efficiency, peak pressure in cylinder, and net heat release rate of engine. Wang et al.[29] compared the accuracy of three machine learning algorithms to predict emissions and fuel consumption of a Wanker rotor engine. The results showed that different models have different advantages, among which the GPR model had very good generalization ability in scarce data sets.

Many researchers use intelligent algorithms to predict engine performance and emission characteristics under different operating conditions[30,31] and use optimization algorithms to find the optimal fuel economy point or Pato boundary[32] with minimum emissions and maximum fuel economy, providing direction for engine calibration, energy conservation, and emission reduction. It can be seen that accurate prediction of engine characteristics plays an important role. However, there are still many shortcomings in previous research, as shown in the following: first, in the past, most researchers only used a single fitting algorithm or compared the prediction accuracy of different algorithms, but few people combined the advantages of various fitting algorithms to optimize the algorithm to seek the maximum determination coefficient and the minimum error.[33] Second, the current modeling methods are mainly applied to light single cylinder engines,[34] with relatively few applications in heavy dual fuel engines and even less in multicylinder heavy diesel/NG dual fuel engines. Finally, researchers used less data in the past and lacked a comparison of the impact of different input states on model predictions.[35]

Based on the abovementioned limitations, this study considers engine speed, torque, NG substitution rate (NGSR), diesel injection pressure (DIP), and diesel injection timing (DIT) as input parameters of the model and heat release (CA50), brake-specific fuel consumption (BSFC), brake thermal efficiency (BTE), CO, CO_2, total unburned hydrocarbon (THC), NO_x, and soot as output parameters of the model. Subsequently, a coupled Gaussian process regression and feedback neural network (GPR-FNN) prediction model was built based on a six-cylinder heavy-duty diesel/NG dual-fuel engine to predict the performance and emission characteristics of the engine. Finally, the GPR-FNN model was used to predict those parameters that did not appear in the training set but were close to the training set data for verification, and contour plots were used to compare the predicted results with the experimental results. The innovations highlighted in this study are summarized as follows:

- An GPR-FNN prediction model was established based on a six-cylinder heavy-duty diesel/NG dual-fuel engine.
- The parameters affecting engine performance were fully considered, and the output parameters were relatively comprehensive.
- For multiparameter inputs, each parameter was output separately, which improved the accuracy of the GPR-FNN model predictions.
- Graphs were used to visually compare predicted and experimental results on performance and emission characteristics

2. EXPERIMENTAL DEVICE AND METHOD

2.1. Experimental Device. For the experiment, we used a six-cylinder, 10.338 L displacement, and 265 kW direct-injection diesel engine. The main technical parameters of the test engine are presented in Table 1. To achieve diesel/NG dual-fuel combustion without changing the original diesel supply system, an NG supply system was added to the periphery. Figure 1 shows the relationship between the test engine, NG supply system, and peripheral test equipment. During the test, to facilitate the adjustment of parameters, the INCA V7.0 software package of ETAS was used to communicate with the ECU, and the working conditions of the engine were changed by adjusting parameters such as engine speed, fuel-injection advance angle, and NG substitution rate. In addition, an eddy current dynamometer was used to obtain basic information, such as engine speed, torque, and power. The emissions of NO_x, THC, CO, and CO_2 were measured using a Horiba MEXA 7100DEGR instrument, and soot emissions were measured using an AVL 415SE smoke meter.

Table 1. Main Technical Parameters of the Experimental Engine

item/unit	specifications
number of cylinder	6
displacement/L	10.338
compression ratio	17.5
bore/mm	123
stroke/mm	145
rated power/kW	265 (1900 r/min)
maximum torque/N·m	1700 (1200−1500 r/min)

The sensitivity and uncertainty analyses of the various measuring instruments used in this study can be found in ref 36. During the test, to improve the test-data accuracy, cooling water temperature was controlled at 87 ± 1 °C, and the intake air temperature was controlled at 24 ± 1 °C. Multiple tests were performed under the same working conditions to ensure the stability of the tests. Regular maintenance of the test equipment and instruments was performed, and the errors of the related instruments can be seen in ref 37. Among them, the calculation formulas for NGSR and BTE are expressed in eqs 1 and 2, respectively.

$$\mathrm{NGSR} = \frac{m_{\mathrm{NG}} H_{\mathrm{NG}}}{m_{\mathrm{NG}} H_{\mathrm{NG}} + m_{\mathrm{diesel}} H_{\mathrm{diesel}}}, \quad (1)$$

$$\mathrm{BTE} = \frac{3600^{*} P_e}{m_{\mathrm{NG}} H_{\mathrm{NG}} + m_{\mathrm{diesel}} H_{\mathrm{diesel}}}, \quad (2)$$

where m_{NG} (kg/h) represents natural gas consumption, m_{diesel}(kg/h) represents diesel consumption, H_{NG} (J/kg) represents low calorific value of natural gas, H_{diesel} (J/kg) represents low calorific value of natural gas, and P_e (W) represents effective power.

https://doi.org/10.1021/acsomega.3c01636
ACS Omega 2023, 8, 18212−18224

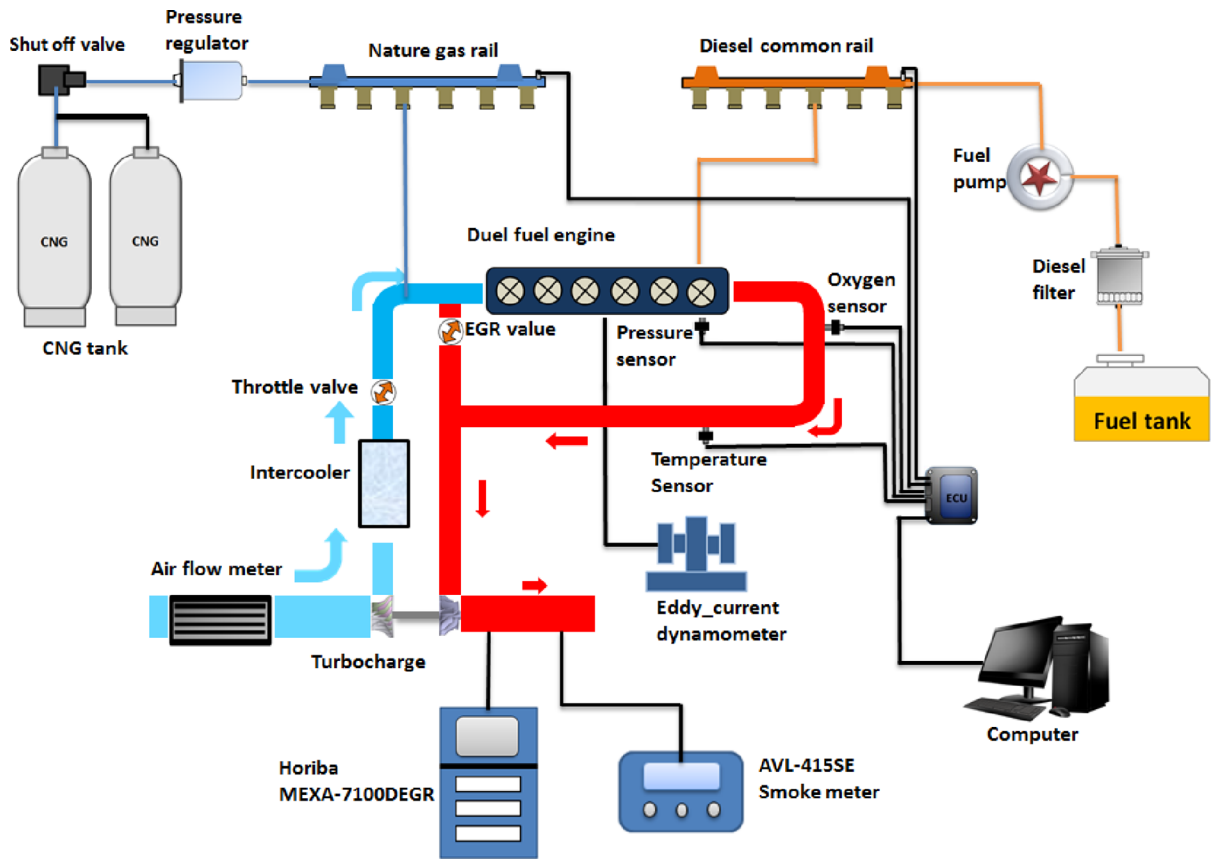

Figure 1. Layout of the test.

Table 2. Factors Considered and Their Chosen Levels

	levels				
factor or input parameters/unit	I	II	III	IV	V
speed/rpm	1220	1720			
torque/N·m	400	800	1200		
NG substitution rate/%	65	75	85	95	
injection pressure/bar	800	1000	1200	1400	1600
injection timing/(° CA ATDC)	-15	−12	−9	−6	−3

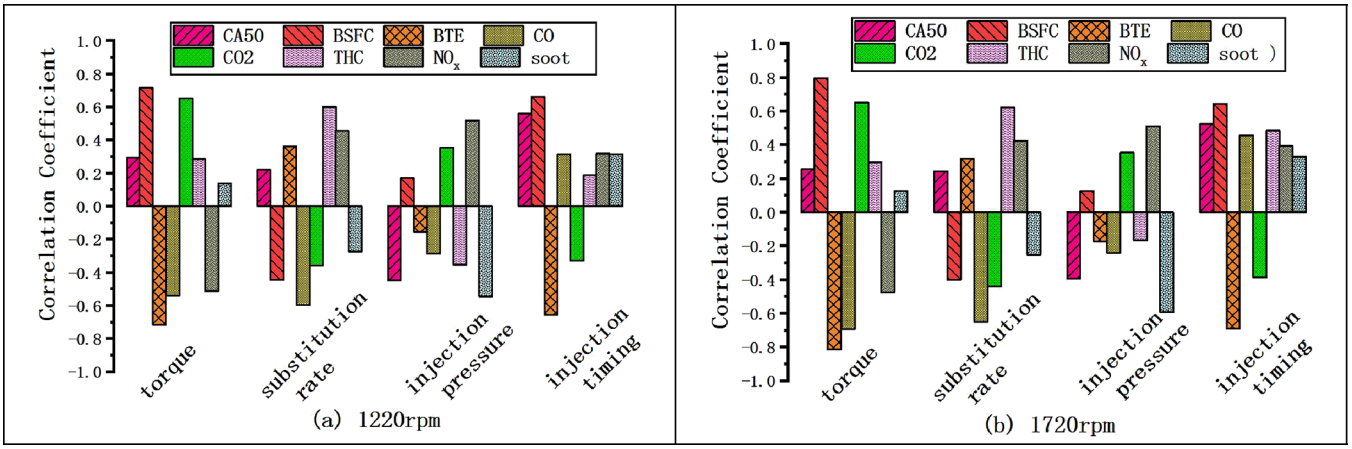

Figure 2. Correlation between input and output parameters at different engine speeds: (a) speed = 1220 rpm; (b) speed = 1720 rpm.

https://doi.org/10.1021/acsomega.3c01636
ACS Omega 2023, 8, 18212−18224

3. GPR-FNN MODEL

3.1. Selection of Input and Output Parameters. This study chose a multilevel design approach with different factors.[38] The different factors and their respective grades are listed in Table 2. It can be concluded from the table that 600 sets of tests were conducted under different working conditions. In addition, the experiment also tested the engine emission and combustion characteristics at a speed of 1420 rpm, torque of 800 N. m, and rail pressure of 1400 bar to verify the accuracy of the established model. Further details are provided in Section 5.

It is well known that the choice of input parameters significantly affects the accuracy of GPR-FNN fitting data. In this study, using the engine speed, torque, NGSR, DIP, and DIT as input parameters, a GPR-FNN model was established to predict the performance and emission performance of an engine. Among them, the CA50, BSFC, and BTE were used for engine performance evaluations, and the CO, CO_2, THC, NO_x, CH_4, and soot emissions were used as engine emission-performance indicators.

As the Pearson linear correlation coefficient is the most commonly used correlation coefficient,[39] it was used to understand the dependence strength of each output feature on a given input, that is, the sensitivity. In other words, this analysis could effectively identify changes in the intended target by changing the input variables alone.[40] The Pearson correlation coefficient is defined using eq 3.

$$\mathrm{Cov}(A, B) = \frac{\sum_{i=1}^{n} (X_{a,i} - \bar{X}_a)(Y_{b,i} - \bar{Y}_b)}{\left\{ \sum_{i=1}^{n} (X_{a,i} - \bar{X}_a)^2 \sum_{j=1}^{n} (Y_{b,j} - \bar{Y}_b)^2 \right\}^{0.5}}, \quad (3)$$

where X_a represents columns in matrix A, Y_b represents columns in matrix B, $\bar{X}_a = \sum_{i=1}^{n} (X_{a,i})/n$ represents the average of column X_a, $\bar{Y}_b = \sum_{j=1}^{n} (Y_{b,j})/n$ represents the average of column Y_b, and n represents the length of the column.

In this study, the Pearson correlation matrix was used to calculate the Pearson correlation between the input variables and the expected output variables of the engine at two speeds, and the results are shown in Figure 2. In general, the value range of the Pearson coefficient is between $[-1, 1]$. When the value of the Pearson coefficient is less than zero, the correlation is negative, whereas a value greater than zero indicates a positive correlation. The closer the absolute value of the Pearson coefficient is to 1, the more the output is affected by the input. The closer it is to zero, the less the input affects the output. When it is equal to zero, the input variables have no effect on the output response, that is, they are independent of each other.[41,42]

As shown in Figure 2, the torque, NGSR, DIP, and DIT had the same effects on the CA50, BSFC, BTE, CO, CO_2, THC, NO_x, and soot at different speeds.[43−45] For determining the combustion characteristics of the engine, the DIT is an important factor. However, for the fuel economy, the NGSR and DIP are relatively unimportant, and for the emission characteristics, the DIT exerts a small impact.[46]

3.2. GPR-FNN Model Structure. *3.2.1. FNN Modeling.* FNN can be used for modeling, classification, estimation, or optimization. A neural network is an extensive parallel, interconnected network of simple adaptive units that are organized to simulate the interaction of biological nervous systems with real-world objects. An FNN is based on data-driven methods, such that an appropriate learning algorithm can be employed to correlate the known input and output data.[47]

In general, the structure of an FNN mainly consists of three parts: an input layer, a hidden layer, and an output layer.[48] The hidden layer can contain one or more layers. Because this study used the engine speed, torque, NGSR, DIP, and DIT as the input parameters, there were five input layers. To improve the accuracy of the FNN prediction model, the CA50, BSFC, BTE, and CO, CO_2, THC, NO_x, and soot emissions were used as the output parameters; therefore, the model contained eight

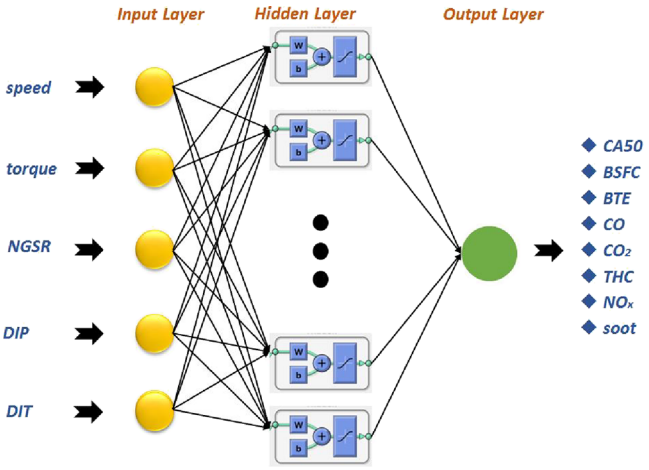

Figure 3. Schematic of the FNN model structure.

Table 3. Software Parameter Configurations

MATLAB	parameter configurations
topology	5 input layers, 8 different outputs, two hidden layers, the hidden layer size is 15, which is 8 (5-15-15-1)
training function	gradient descent with momentum (traingdm)
transfer function	logarithmic sigmoid (logsig)
learning function	gradient descent with momentum (learngdm)

different output layers. In summary, the FNN model established in this study contained five input layers, eight different output layers, and two hidden layers, of which the hidden layer size was 15, that is, 8 (5-15-15-1). A schematic of the FNN model structure is shown in Figure 3. Table 3 lists the detailed FNN settings.

3.2.2. GPR Modeling. In recent years, GPR has been widely used in engineering applications because of their effectiveness in defining arbitrary functions and solving complex problems. GPR is a supervised learning method based on the Bayesian framework, which has strict theoretical logic and is very suitable for dealing with small samples, nonlinear, and other complex regression problems. The GPR model is widely used in engine calibration because it is easy to implement and automatically solve super parameters. In the function space, a GP is completely described by the mean function and covariance function, so GP is also denoted as GP(mean,cov), where mean is the mean function and cov is the covariance function, also known as the kernel function. Commonly used kernel functions include exponential kernel, square exponential kernel, etc., whose definition is as follows:

Exponential kernel function

https://doi.org/10.1021/acsomega.3c01636
ACS Omega 2023, 8, 18212−18224

$$k(x_i, x_j|\theta) = {\sigma_f}^2 \exp\left(-\frac{r}{\sigma_l}\right) \quad (4)$$

Square exponential kernel function

$$k(x_i, x_j|\theta) = {\sigma_f}^2 \exp\left[-\frac{1}{2}\frac{(x_i - x_j)^T(x_i - x_j)}{{\sigma_l}^2}\right] \quad (5)$$

Table 4. Software Parameter Configurations

MATLAB	parameter configurations
kernel function	squared exponential function
prediction method	nearly complete independence
evaluation method	accurate GPR fitting
transfer function	logarithmic sigmoid (logsig)
maximum number of iterations	1×10^6

where σ_l represents the characteristic length, σ_f represents the standard deviation, x_i and x_j represent the predicted value, and $r = \sqrt{(x_i - x_j)^T(x_i - x_j)}$ represents the Euclidean distance.

In order to improve the prediction accuracy of the model, before GPR modeling, kernel parameters and σ were first optimized automatically using the iterative method, and then the GPR model was established by assigning the solved parameters as the initial parameters. Table 4 describes the GP parameters.

3.2.3. Model Coupling. By coupling the two trained models together, the new model was characterized by the maximum coefficient of determination (R^2) and minimum relative average absolute error (RAAE). Let the coefficient of GPR be m and the coefficient of FNN be n and establish the coefficient of bivariate primary equation so that the equation satisfies [max(R^2),min-(RAAE)] = $m \times$ GPR + $n \times$ FNN. As can be seen from the definition of GPR-FNN, Compared to other single fitting algorithms, this algorithm combines the advantages of other algorithms and finally makes R^2 maximum and the error minimum. The algorithm has the following advantages: first, the algorithm optimizes the fitting function itself, making the global accuracy highest; second, the advantages of each algorithm are recorded and amplified. Finally, the algorithm can compensate the points with poor local prediction performance. The definitions of R^2 and RAAE are shown in eqs 6 and 7:

$$R^2 = \frac{\left(n\sum_{i=1}^n \hat{y}_i y_i - \sum_{i=1}^n \hat{y}_i \sum_{i=1}^n y_i\right)^2}{\left(n\sum_{i=1}^n \hat{y}_i^2 - \left(\sum_{i=1}^n \hat{y}_i\right)^2\right)\left(n\sum_{i=1}^n y_i^2 - \left(\sum_{i=1}^n y_i\right)^2\right)} \quad (6)$$

$$\mathrm{RAAE} = \frac{\sum_{i=1}^n |y_i - \hat{y}_i|}{n \times \mathrm{STD}} = \frac{\mathrm{mean}(|y_i - \hat{y}_i|)}{\mathrm{STD}} \quad (7)$$

where y_i represents the actual value, $\hat{y}_i$ represents the predicted value, and n represents the total number of samples; STD represents the standard deviation. Larger R^2 means more accuracy and lower RAAE values indicate more accuracy.

4. FORECAST RESULTS AND ERROR ANALYSIS

4.1. Prediction Results. Based on experiments, a GPR-FNN was built to predict CA50, BSFC, BTE, and the CO, CO, THC, NO_x, and soot emissions, where speed, torque, NGSR, DIP, and DIT were used as the input parameters. The R-values of the output parameters in training, testing, validation, and all cases were obtained, as presented in Table 5. As observed from the table, the smallest R-value appeared in the CA50 test, which was 0.98326, and the largest R-value appeared in the training dataset of BSFC, which was 0.99738.

Table 5. Comprehensive *R*-Values

output	training	validation	test	all
CA50	0.99474	0.98634	0.98326	0.99204
BSFC	0.99738	0.99569	0.99211	0.99608
BTE	0.99676	0.99406	0.98874	0.99549
CO	0.99862	0.98683	0.99197	0.99566
CO_2	0.99613	0.98818	0.99236	0.99444
THC	0.99511	0.99444	0.99069	0.99421
NO_x	0.99253	0.98814	0.99065	0.99245
soot	0.99554	0.99394	0.99440	0.99511

Figure 4 shows the fitting of the experimental values of all output parameters and the predicted values of the GPR-FNN. The black line represents the best-fitting result. Evidently, the predicted value is equal to the experimental value, indicating that the GPR-FNN can accurately predict the experimental result. According to Figure 4, the overall R-value of all the output parameters is greater than 0.995. The correlation coefficients R of CA50, BSFC, BTE, CO, CO_2, THC, NO_x, and soot were 0.99204, 0.99608, 0.99549, 0.99566, 0.99444, 0.99421, 0.99322, and 0.99511, respectively. The R-value of BSFC was at most 0.99608, and the R-value of CA50 was 0.99608. The minimum value was 0.99204.

4.2. Error Analysis. There are several indicators for evaluating the GPR-FNN prediction results. Commonly used technical indicators for error analysis include the mean square error, root mean square error, mean absolute error, SMAPE, MSRE, and MAPE. Among them, mean square error, root mean square error, and mean absolute error are absolute errors, and SMAPE, MSRE, and MAPE are relative errors. In this study, relative error was used as a technical indicator to discuss the deviation between the GPR-FNN prediction and the experimental results. The definitions of SMAPE, MSRE, and MAPE are expressed in eqs 8−10, respectively. By definition, MSRE is the square of the relative error. The main difference between SMAPE and MAPE is in the denominator, where SMAPE takes the average of the absolute values of the prediction and experiment as the denominator and MAPE takes the absolute value of the experiment as the denominator.

The relative error was calculated from the experimental and predicted data, as shown in Figure 5. As shown in the figure, all statistical errors were less than 6.5%; among them, the MAPE of CA50, BSFC, BTE, CO, CO_2, THC, NO_x, and soot were 4.051, 1.606, 1.934, 5.692, 3.334, 5.861, 5.668, and 4.87%, respectively. The MAPE of THC was the largest at 5.861%, and the MAPE of BSFC was the smallest at 1.606%, whereas both SMAPE and MSRE were less than 1.5%.

$$\mathrm{SMAPE} = \frac{1}{n}\sum_{i=1}^n \frac{|\hat{y}_i - y_i|}{(|\hat{y}_i| + |y_i|)/2} \quad (8)$$

$$\mathrm{MSRE} = \left|\frac{1}{n}\sum_{i=1}^n \frac{(\hat{y}_i - y_i)^2}{\hat{y}_i^2}\right| \quad (9)$$

https://doi.org/10.1021/acsomega.3c01636
ACS Omega 2023, 8, 18212−18224

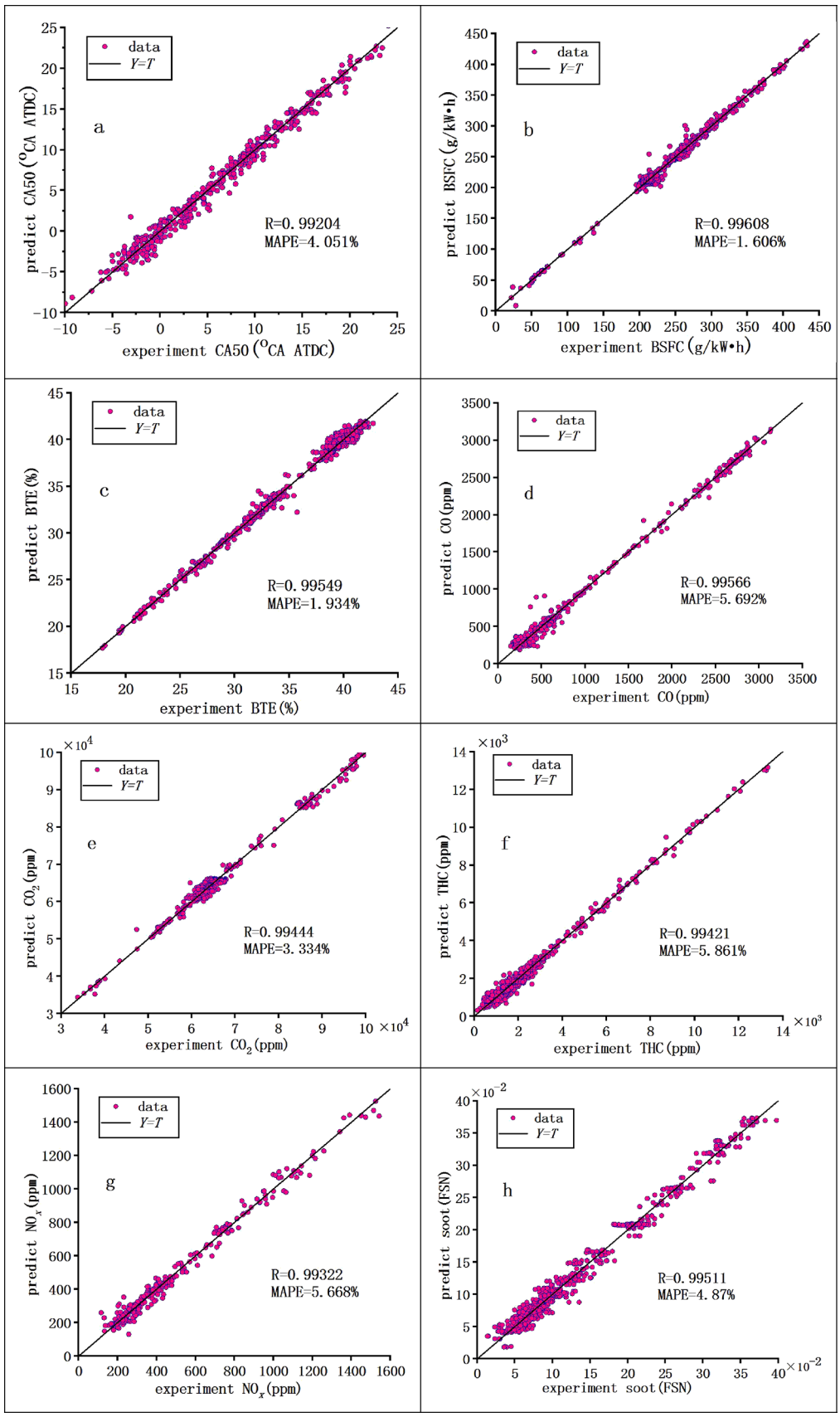

Figure 4. Corresponding relationship between experimental data and predicted data: (a) CA50, (b) BSFC, (c) BTE, (d) CO, (e) CO_2, (f) THC, (g) NO_x, (h) FSN.

https://doi.org/10.1021/acsomega.3c01636
ACS Omega 2023, 8, 18212−18224

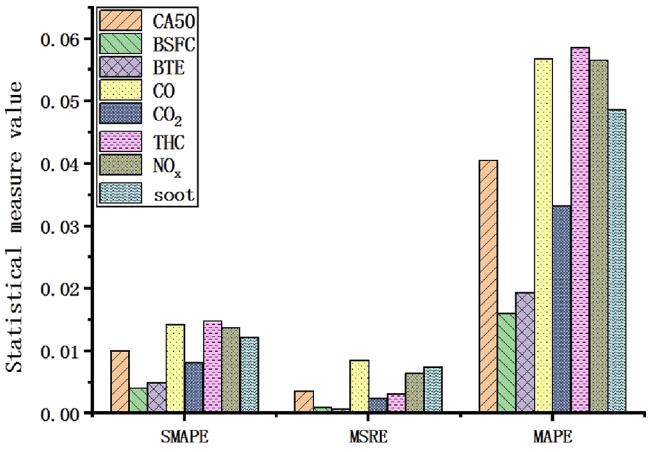

Figure 5. Error variations.

$$\mathrm{MAPE} = \frac{1}{n}\sum_{i=1}^{n}\left|\frac{\hat{y}_i - y_i}{y_i}\right| \quad (10)$$

where y represents the actual value; $\hat{y}$ represents the predicted value; and n represents the total number of samples.

5. VALIDATION OF GPR-FNN PREDICTION RESULTS

Because the establishment of the GPR-FNN model is similar to the black-box operation,[49] to observe the difference between the prediction and the test results easily, this paper mainly discusses the engine performance, emissions, and different NGSRs of the engine under the operating conditions of 1420 rpm, 800 N. m, a DIP of 1400 bar (65%−90%), and a DIT between −12° CA ATDC and −3° CA ATDC. To compare the GPR-FNN prediction results with the corresponding test data for CA50, BSFC, BTE, CO, CO_2, THC, NO_x, and soot, contour maps were used, which show the relationship between engine performance and emissions, NGSR, and DIT, as shown in Figures 6−13, respectively.

As shown in Figure 6, if NGSR remained constant, CA50 was delayed as the injection advance angle decreases. Under the same DIT conditions, with an increase in NGSR, CA50 showed a trend of advancing first and then delaying. When the NGSR was 90% and DIT was −4° CA ATDC, CA50 was delayed by 9° CA ATDC, which had an adverse effect on combustion. In addition, when NGSR was lower than 80%, the relationship between CA50 and DIT was linear. When NGSR was greater than 85%, the combustion speed decreased, and CA50 was further delayed at the same DIT value. For CA50, the main difference between the experimental and the predicted results was in the NGSR between 70% and 75%. When the DIT was earlier than −10° CA ATDC, the predicted CA50 was earlier than the experimental data.

As shown in Figure 7, in the case of a small NGSR (less than 70%), the BSFC decreased with an increase in the DIT. When the NGSR was 65% and DIT was −4° CA ATDC, the BSFC was the smallest, approximately 215 g/kW·h. As observed from Figure 8, the BTE was the largest at this point; therefore, the fuel economy was the best at this point. In the case of a larger DIT (greater than −6° CA ATDC), the BSFC exhibited two maximum points with an increase in the NGSR, and the corresponding NGSR values were 75 and 90%. By comparing the test results with the prediction results, it was found that the main differences were the following: (1) the GPR-FNN predicted values were too large when the NGSR and injection advance angle were small. (2) When DIT was −9° CA ATDC, the NGSR was between 83 and 87%, which indicates a low prediction value.

As observed from Figure 8, when the NGSR was unchanged, the BTE increased with the increase in the DIT, and when the DIT was unchanged, the BTE decreased with the increase in the NGSR. In the case of a small NGSR (65%) and a small injection advance angle (4° CA ATDC), the BTE was the largest, and the engine exhibited good fuel economy. In the case of a large NGSR and a large injection advance angle (12° CA ATDC), the fuel economy was poor.

As observed from Figure 9, when the DIT was unchanged, the CO emissions first showed a rapidly decreasing trend; subsequently, it showed an increasing trend, and finally, it showed a decreasing trend with an increase in the NGSR. In the case of a large NGSR (greater than 70%), the DIT had little effect on CO emissions. Under a small NGSR, CO emissions

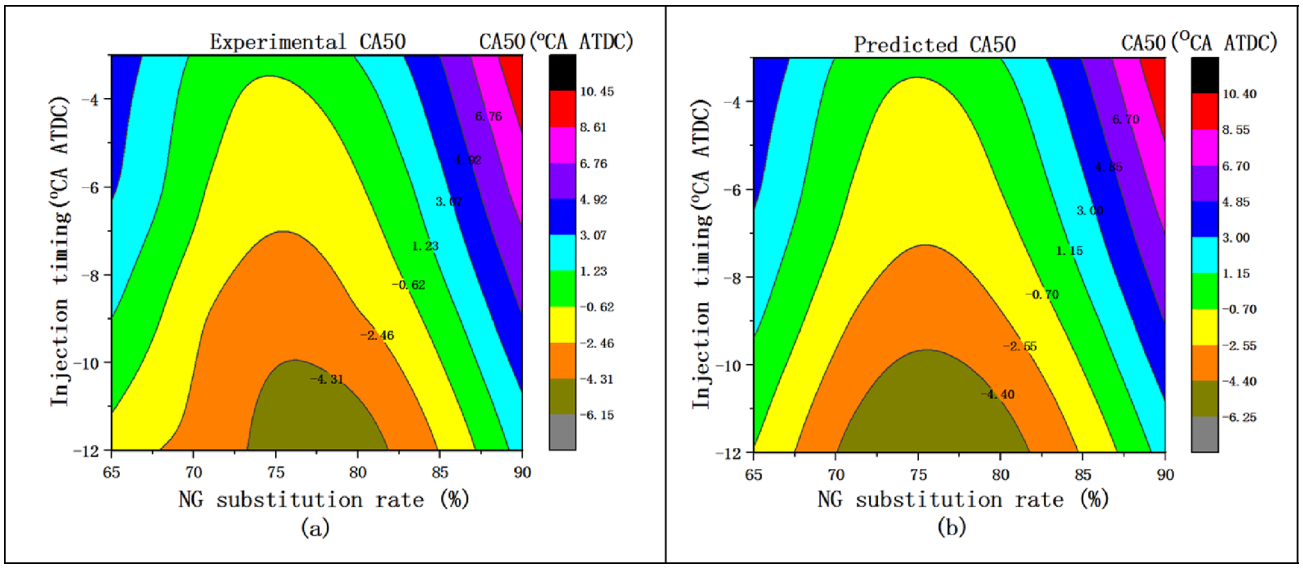

Figure 6. Comparison of CA50 predicted by GPR-FNN with experimental data: (a) experimental result; (b) predicted result.

https://doi.org/10.1021/acsomega.3c01636
ACS Omega 2023, 8, 18212−18224

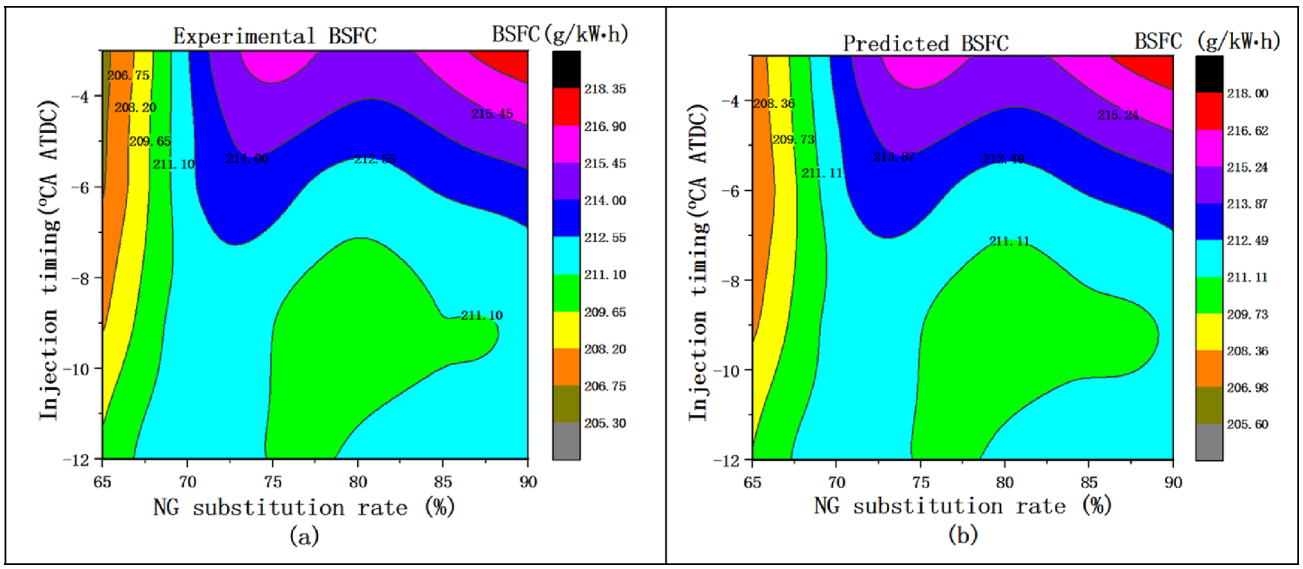

Figure 7. Comparison of BSFC predicted by GPR-FNN with experimental data: (a) experimental result; (b) predicted result.

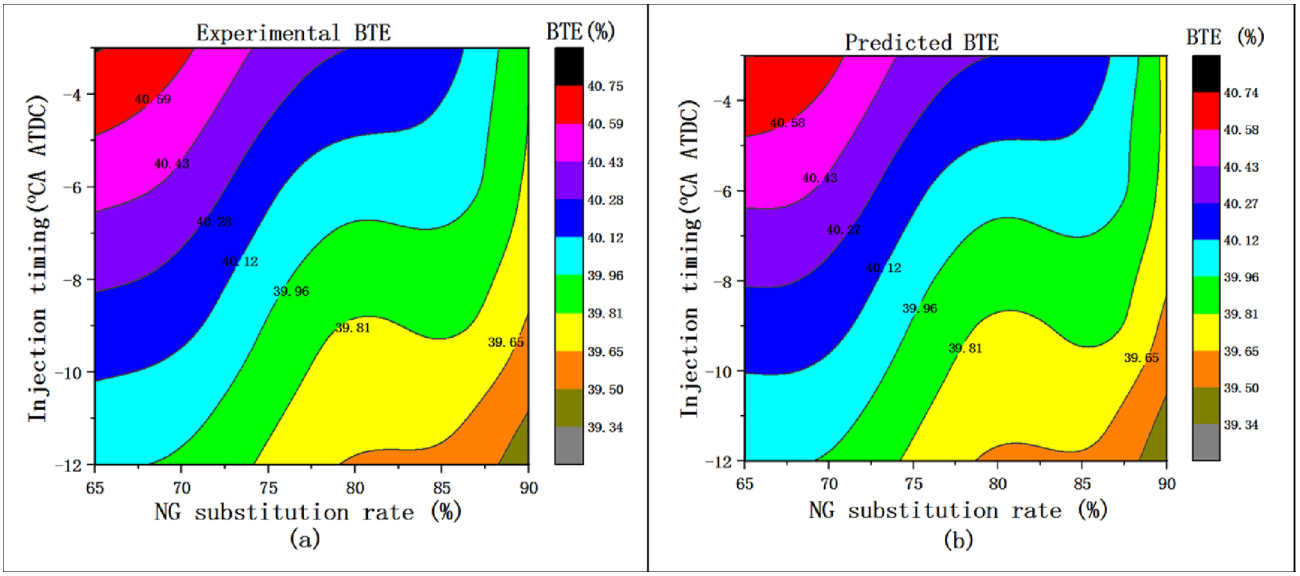

Figure 8. Comparison of BTE predicted by GPR-FNN with experimental data: (a) experimental result; (b) predicted result.

decreased with an increase in DIT. When the NGSR was 65% and the NGSR was −12° CA ATDC, the CO emission was the highest at 540 ppm. When the NGSR was 73%, the CO emission was the lowest at 210 ppm.

As observed from Figure 10, when the DIT was unchanged, the CO_2 emissions decreased with an increase in the NGSR. When the NGSR was 90% and DIT was −4° CA ATDC, the amount of CO_2 emission was the smallest at approximately 58,500 ppm. When the NGSR was less than 68%, the DIT was between −11° CA ATDC and − 4° CA ATDC, and the amount of CO_2 emission was the largest at approximately 67,000 ppm. With an increase in the NGSR, the main reasons for the decrease in CO_2 are as follows: first, the C/H of NG is lower, and the CO_2 produced by NG combustion is less; second, the injection advance angle is smaller, the diesel used for piloting is less, and the cylinder temperature is higher. Therefore, CO could not be completely converted into CO_2. Comparing the test results with the predicted results, it was found that the predicted CO_2 emission value was slightly small, and the relative error was within 2%.

As observed from Figure 11, by keeping the injection time unchanged, the THC emission first decreased and then increased with an increase in the NGSR, and the lowest THC emission was 575 ppm when the NGSR was approximately 72%. When the NGSR was less than 76%, the THC emission decreased with a decrease in the injection advance angle, whereas when the NGSR was greater than 76%, the fuel injection advance angle had little effect on the THC emission. When the NGSR was greater than 75%, the THC emissions increased with an increase in the NGSR. The main reasons can be attributed to the following two points: first, the main component of NG is CH_4, and therefore, the amount of THC in the emission increases. Second is the high compressibility of NG; therefore, when a large amount of NG is compressed into the combustion-chamber gap, it does not participate in combustion and causes the main THC emissions. In the case of THC, the main difference between the experimental and the

https://doi.org/10.1021/acsomega.3c01636
ACS Omega 2023, 8, 18212−18224

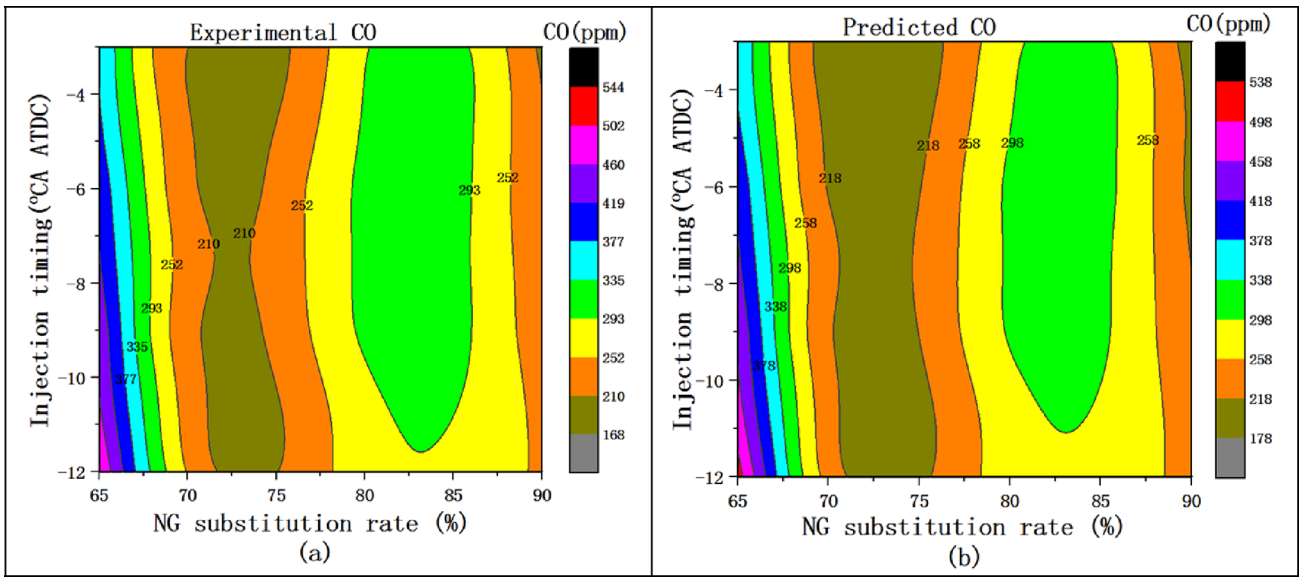

Figure 9. Comparison of CO predicted by GPR-FNN with experimental data: (a) experimental result; (b) predicted result.

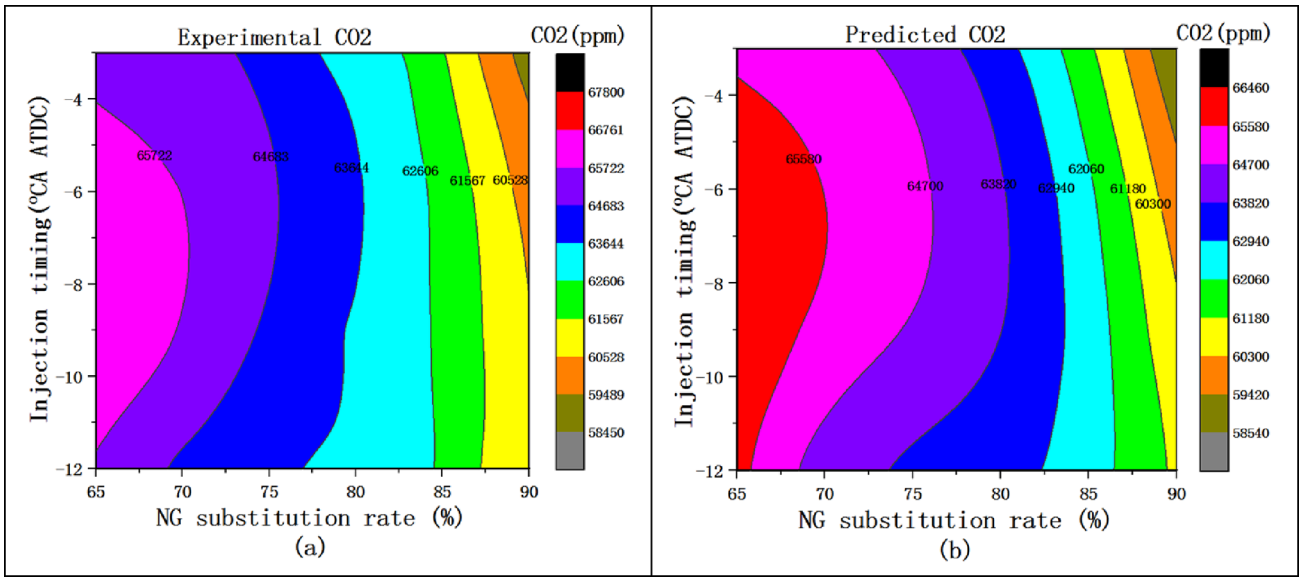

Figure 10. Comparison of CO_2 predicted by GPR-FNN with experimental data: (a) experimental result; (b) predicted result.

predicted results was that the NGSR was approximately 78%. When the DIT was earlier than −10° CA ATDC, the predicted THC emissions were smaller than that of the experiments.

The three main factors affecting NO_x emissions are high temperature, oxygen enrichment, and high-temperature duration. As observed from Figure 12, when the NGSR remained constant, the NO_x emissions decreased with a decrease in the injection advance angle. The main reason is that with a decrease in the DIT, the amount of diesel fuel ignited decreases, such that the energy released by the premixed combustion of diesel and NG is low, resulting in a low combustion temperature in the cylinder. At the same injection time, the NO_x emissions first remained constant and then decreased with an increase in the NGSR, and when the NGSR was greater than 80%, it exhibited a linear relationship with the NGSR. Combined with Figure 6, the main reason is that when the NGSR was greater than 80%, the CA50 was delayed, and the high-temperature duration was reduced. A comparison showed that the experimental results were consistent with the predicted results, and the relative error between the two was within 1%.

As shown in Figure 13, by keeping the NGSR constant, the soot emission increased with a decrease in the injection advance angle. Compared to Figure 12, the trend of the soot emission was opposite to that of the NO_x emission,[50] which shows a trade-off between soot and NO_x. When the NGSR was greater than 73% and the DIT was −4° CA ATDC, the soot emission was the highest at approximately 0.306 FSN, and when the NGSR was less than 77% and the DIT was −12° CA ATDC, the soot emission was the lowest at approximately 0.112 FSN. In the case of soot emission, the main difference between the test and the predicted results was that the NGSR was approximately 85%, and the soot emissions obtained from the test results were higher.

From the above analyses, it can be observed that the GPR-FNN prediction results are highly accurate.

https://doi.org/10.1021/acsomega.3c01636
ACS Omega 2023, 8, 18212−18224

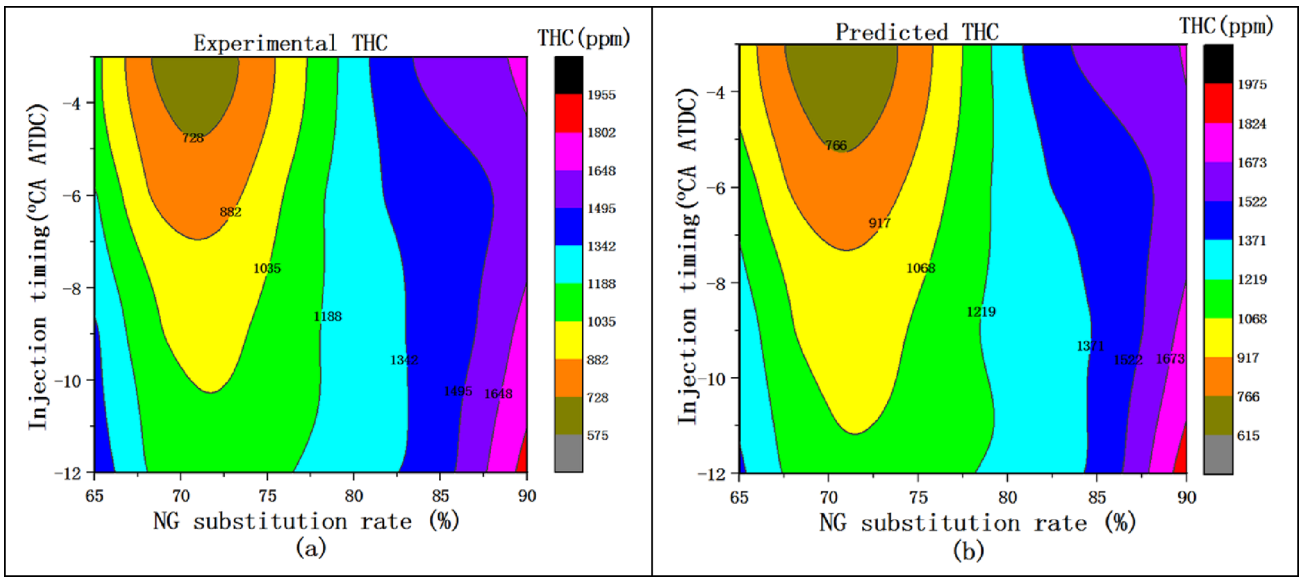

Figure 11. Comparison of THC predicted by GPR-FNN with experimental data: (a) experimental result; (b) predicted result.

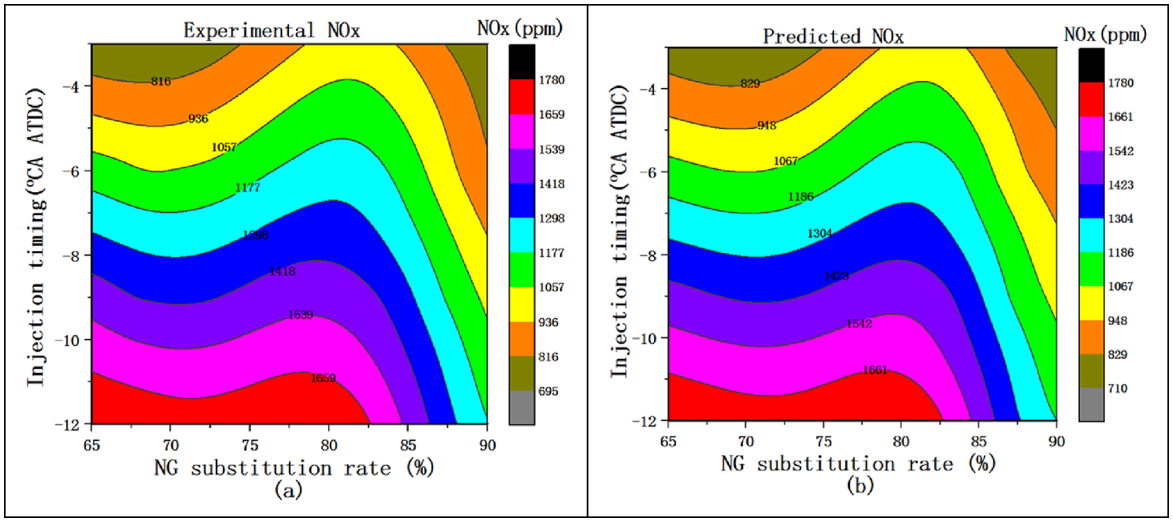

Figure 12. Comparison of NO_x predicted by GPR-FNN with experimental data: (a) experimental result; (b) predicted result.

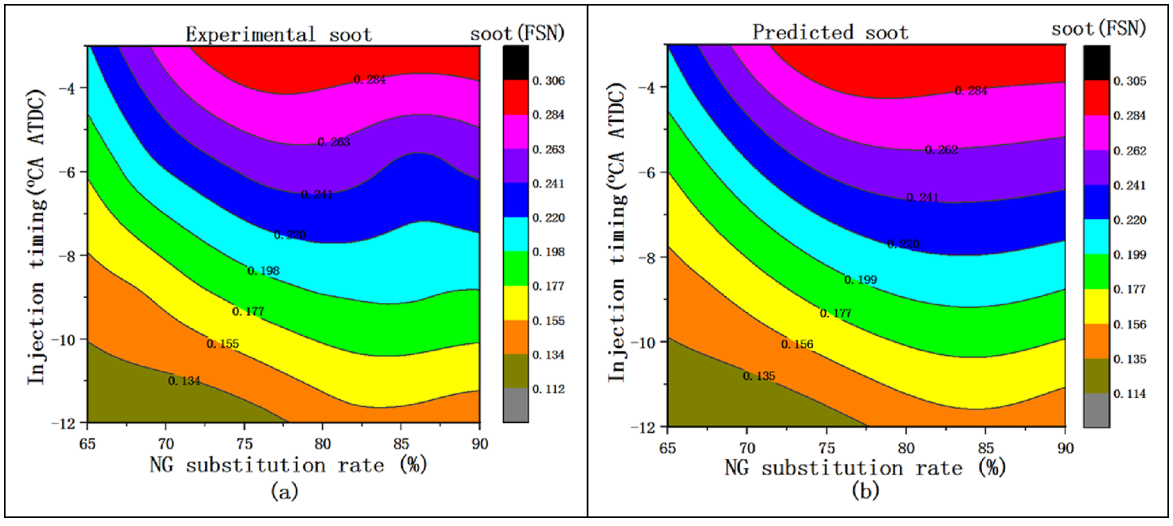

Figure 13. Comparison of soot predicted by GPR-FNN with the experimental data: (a) experimental result; (b) predicted result.

https://doi.org/10.1021/acsomega.3c01636
ACS Omega 2023, 8, 18212−18224

6. CONCLUSIONS

In this study, a GPR-FNN model was developed to predict the performance and emission performance of a six-cylinder heavy-duty diesel/NG dual-fuel engine. Considering the engine speed, torque, NGSR, DIP, and DIT as input parameters, this study constructed a GPR-FNN model for predicting the CA50, BSFC, BTE, CO, CO_2, THC, NO_x, and soot emissions. The proposed GPR-FNN model was evaluated using relative error and performance metrics and was validated experimentally. The main findings of this study are as follows:

(1) Pearson correlation analysis was performed on the input and output parameters, and it was concluded that for the performance of the engine, the DIT is an important factor. The NGSR and DIP are relatively unimportant for the fuel economy, and for the emission characteristics, the DIT exerts less influence.

(2) A GPR-FNN engine performance and emission prediction model was established. Overall, the GPR-FNN prediction values had high accuracy, with the *R*-value between 0.99204 (CA50) and 0.99608 (BSFC), MAPE between 1.606 (BSFC) and 5.861% (THC), and both SMAPE and MSRE values being less than 1.5%.

(3) The GPR-FNN prediction model was verified experimentally, and it was found that the predicted results were close to the test results. This shows that the GPR-FNN can accurately predict the diesel/NG dual-fuel engine performance and emissions.

AUTHOR INFORMATION

Corresponding Author

Haozhong Huang − *College of Mechanical Engineering, Guangxi University, Nanning 530004, China;* orcid.org/0000-0001-7181-3840; Email: hhz421@gxu.edu.cn

Authors

Jialong Li − *College of Mechanical Engineering, Guangxi University, Nanning 530004, China*

Taoming Wan − *College of Mechanical Engineering, Guangxi University, Nanning 530004, China*

Guixin Chen − *College of Mechanical Engineering, Guangxi University, Nanning 530004, China*

Jianguo Liang − *College of Mechanical Engineering, Guangxi University, Nanning 530004, China*

Baijun Lei − *College of Mechanical Engineering, Guangxi University, Nanning 530004, China*

Complete contact information is available at: https://pubs.acs.org/10.1021/acsomega.3c01636

Notes

The authors declare no competing financial interest.

ACKNOWLEDGMENTS

This work is supported by the Guangxi Science and Technology Major Project (AA22068103) and the Guangxi Key R&D Program (AB21220055).

NOMENCLATURE

GPR-FNN	coupled Gaussian process regression and feedback neural network algorithm
NG	natural gas
CA50	crank angle corresponding of 50% heat release
BSFC	brake specific fuel consumption
BTE	brake thermal efficiency
CO	carbon monoxide
CO_2	carbon dioxide
THC	total unburned hydrocarbon
NO_x	oxides of nitrogen
R	regression correlation coefficients
R^2	coefficient of determination
RAAE	relative average absolute error
MAPE	mean absolute percentage error
MSRE	mean square relative error
SMAPE	symmetric mean absolute percentage error
ATDC	after top dead center
NGSR	natural gas substitution rate
DIP	diesel injection pressure
DIT	diesel injection timing

REFERENCES

(1) Zhang, C.; Li, Y.; Liu, Z.; Liu, J. An investigation of the effect of plateau environment on the soot generation and oxidation in diesel engines. *Energy* **2022**, *253*, No. 124086.

(2) Jiang, Z.; Rahman Mahmud, A.; Maneengam, A.; Nassani, A. A.; Haffar, M.; Cong, P. T. Non linear effect of Biomass, fossil fuels and renewable energy usage on the economic Growth: Managing sustainable development through energy sector. *Fuel* **2022**, *326*, No. 124943.

(3) Shi, C.; Ji, C.; Ge, Y.; Wang, S.; Bao, J.; Yang, J. Numerical study on ignition amelioration of a hydrogen-enriched Wankel engine under lean-burn condition. *Appl. Energy* **2019**, *255*, No. 113800.

(4) Yin, X.; Li, W.; Zhang, W.; Lv, X.; Yang, B.; Wang, Y.; Zeng, K. Experimental analysis of the EGR rate and temperature impact on combustion and emissions characteristics in a heavy-duty NG engine. *Fuel* **2022**, *310*, No. 122394.

(5) Liu, W.; McKibbin, W. J.; Morris, A. C.; Wilcoxen, P. J. Global economic and environmental outcomes of the Paris Agreement. *Energy Economics* **2020**, *90*, No. 104838.

(6) Said, Z.; Le, D. T. N.; Sharma, P.; Dang, V. H.; Le, H. S.; Nguyen, D. T.; Bui, T. A. E.; Nguyen, V. G. Optimization of combustion, performance, and emission characteristics of a dual-fuel diesel engine powered with microalgae-based biodiesel/diesel blends and oxy-hydrogen. *Fuel* **2022**, *326*, No. 124987.

(7) Wang, T.; Chen, R.; Jiang, H.; Qiao, X.; Li, T. Experimental study of soot particles characteristics for hydrous ethanol diesel emulsified fuel under diesel-like conditions. *Fuel Process. Technol.* **2022**, *235*, No. 107384.

(8) Wardana, M. K. A.; Lim, O. Investigation of ammonia homogenization and NOx reduction quantity by remodeling urea injector shapes in heavy-duty diesel engines. *Appl. Energy* **2022**, *323*, No. 119586.

(9) Hasan, A. O.; Osman, A. I.; Al-Muhtaseb, A. H.; Al-Rawashdeh, H.; Abu-jrai, A.; Ahmad, R.; Gomaa, M. R.; Deka, T. J.; Rooney, D. W. An experimental study of engine characteristics and tailpipe emissions from modern DI diesel engine fuelled with methanol/diesel blends. *Fuel Process. Technol.* **2021**, *220*, No. 106901.

(10) Liu, H.; Zhang, X.; Zhang, Z.; Wu, Y.; Wang, C.; Chang, W.; Zheng, Z.; Yao, M. Effects of 2-ethylhexyl nitrate (EHN) on combustion and emissions on a compression ignition engine fueling high-pressure direct-injection pure methanol fuel. *Fuel* **2023**, *341*, No. 127684.

(11) Rosa, J. S.; Telli, G. D.; Altafini, C. R.; Wander, P. R.; Oliveira Rocha, L. A. Dual fuel ethanol port injection in a compression ignition diesel engine: Technical analysis, environmental behavior, and economic viability. *J. Cleaner Prod.* **2021**, *308*, No. 127396.

(12) Vasanthakumar, R.; Loganathan, M.; Chockalingam, S.; Vikneswaran, M.; Manickam, M. A study on the effect of hydrogen enriched intake air on the characteristics of a diesel engine fueled with ethanol blended diesel. *Int. J. Hydrogen Energy* **2023**.

(13) Cui, Y.; Liu, H.; Wen, M.; Feng, L.; Wang, C.; Ming, Z.; Zhang, Z.; Zheng, Z.; Zhao, H.; Wang, X.; et al. Optical diagnostics and chemical kinetic analysis on the dual-fuel combustion of methanol and high reactivity fuels. *Fuel* **2022**, *312*, No. 122949.
(14) Mabadi Rahimi, H.; Jazayeri, S. A.; Ebrahimi, M. Hydrogen energy share enhancement in a heavy duty diesel engine under RCCI combustion fueled with natural gas and diesel oil. *Int. J. Hydrogen Energy* **2020**, *45*, 17975−17991.
(15) Singh, A.; Saxena, M. R.; Maurya, R. K. Investigating a deterministic yet computationally cheap combustion parameter for model predictive control of a CNG-diesel RCCI engine. *Fuel* **2023**, *332*, No. 126059.
(16) Pandey, V.; Badruddin, I. A.; Khan, T. M. Y. Effect of H2 blends with compressed natural gas on emissions of SI engine having modified ignition timings. *Fuel* **2022**, *321*, No. 123930.
(17) Huang, H.; Lv, D.; Zhu, J.; Zhu, Z.; Chen, Y.; Pan, Y.; Pan, M. Development of a new reduced diesel/natural gas mechanism for dual-fuel engine combustion and emission prediction. *Fuel* **2019**, *236*, 30−42.
(18) Park, H.; Shim, E.; Bae, C. Improvement of combustion and emissions with exhaust gas recirculation in a natural gas-diesel dual-fuel premixed charge compression ignition engine at low load operations. *Fuel* **2019**, *235*, 763−774.
(19) Zhang, Z.; Lv, J.; Li, W.; Long, J.; Wang, S.; Tan, D.; Yin, Z. Performance and emission evaluation of a marine diesel engine fueled with natural gas ignited by biodiesel-diesel blended fuel. *Energy* **2022**, *256*, No. 124662.
(20) Bai, F. J. J. S. A Machine Learning Approach for Carbon di oxide and Other Emissions Characteristics Prediction in a Low Carbon Biofuel-Hydrogen Dual Fuel Engine. *Fuel* **2023**, *341*, No. 127578.
(21) Bai, F. J. J. S.; Shanmugaiah, K.; Sonthalia, A.; Devarajan, Y.; Varuvel, E. G. Application of machine learning algorithms for predicting the engine characteristics of a wheat germ oil−Hydrogen fuelled dual fuel engine. *Int. J. Hydrogen Energy* **2022**.
(22) Wang, H.; Ji, C.; Yang, J.; Wang, S.; Ge, Y. Towards a comprehensive optimization of the intake characteristics for side ported Wankel rotary engines by coupling machine learning with genetic algorithm. *Energy* **2022**, *261*, No. 125334.
(23) Mohan, B.; Badra, J. An automated machine learning framework for piston engine optimization. *Applications in Energy and Combustion Science* **2023**, *13*, No. 100106.
(24) Oh, S.; Kim, C.; Lee, Y.; Park, H.; Lee, J.; Kim, S.; Kim, J. Analysis of the exhaust hydrogen characteristics of high-compression ratio, ultra-lean, hydrogen spark-ignition engine using advanced regression algorithms. *Appl. Therm. Eng.* **2022**, *215*, No. 119036.
(25) Cui, Y.; Liu, H.; Wang, Q.; Zheng, Z.; Wang, H.; Yue, Z.; Ming, Z.; Wen, M.; Feng, L.; Yao, M. Investigation on the ignition delay prediction model of multi-component surrogates based on back propagation (BP) neural network. *Combust. Flame* **2022**, *237*, No. 111852.
(26) Fu, J.; Yang, R.; Li, X.; Sun, X.; Li, Y.; Liu, Z.; Zhang, Y.; Sunden, B. Application of artificial neural network to forecast engine performance and emissions of a spark ignition engine. *Appl. Therm. Eng.* **2022**, *201*, No. 117749.
(27) Taghavi, M.; Gharehghani, A.; Nejad, F. B.; Mirsalim, M. Developing a model to predict the start of combustion in HCCI engine using ANN-GA approach. *Energy Convers. Manage.* **2019**, *195*, 57−69.
(28) Alruqi, M.; Sharma, P.; Deepanraj, B.; Shaik, F. Renewable energy approach towards powering the CI engine with ternary blends of algal biodiesel-diesel-diethyl ether: Bayesian optimized Gaussian process regression for modeling-optimization. *Fuel* **2023**, *334*, No. 126827.
(29) Wang, H.; Ji, C.; Shi, C.; Ge, Y.; Meng, H.; Yang, J.; Chang, K.; Wang, S. Comparison and evaluation of advanced machine learning methods for performance and emissions prediction of a gasoline Wankel rotary engine. *Energy* **2022**, *248*, No. 123611.
(30) Sun, X.; Xie, M.; Zhou, F.; Fu, J.; Liu, J. Multi-objective optimization for combustion, thermodynamic and emission characteristics of Atkinson cycle engine using tree-based machine learning and the NSGA II algorithm. *Fuel* **2023**, *342*, No. 127839.
(31) Wang, H.; Ji, C.; Shi, C.; Yang, J.; Ge, Y.; Wang, S.; Chang, K.; Meng, H.; Wang, X. Parametric modeling and optimization of the intake and exhaust phases of a hydrogen Wankel rotary engine using parallel computing optimization platform. *Fuel* **2022**, *324*, No. 124381.
(32) Tong, J.; Li, Y.; Liu, J.; Cheng, R.; Guan, J.; Wang, S.; Liu, S.; Hu, S.; Guo, T. Experiment analysis and computational optimization of the Atkinson cycle gasoline engine through NSGA II algorithm using machine learning. *Energy Convers. Manage.* **2021**, *238*, No. 113871.
(33) Yadav, J.; Venkatesh, P.; Pischinger, S. Application of micro-genetic algorithms to optimize piston bowl geometries for heavy-duty engines running on diesel and 1-Octanol fuels. *Appl. Therm. Eng.* **2023**, *226*, No. 120236.
(34) Alahmer, H.; Alahmer, A.; Alkhazaleh, R.; Alrbai, M. Exhaust emission reduction of a SI engine using acetone−gasoline fuel blends: Modeling, prediction, and whale optimization algorithm. *Energy Rep.* **2023**, *9*, 77−86.
(35) Li, Y.; Zhou, S.; Liu, J.; Tong, J.; Dang, J.; Yang, F.; Ouyang, M. Multi-objective optimization of the Atkinson cycle gasoline engine using NSGA III coupled with support vector machine and back-propagation algorithm. *Energy* **2023**, *262*, No. 125262.
(36) You, J.; Liu, Z.; Wang, Z.; Wang, D.; Xu, Y. Experimental analysis of inert gases in EGR on engine power and combustion characteristics in a stoichiometric dual fuel heavy-duty natural gas engine ignited with diesel. *Appl. Therm. Eng.* **2020**, *180*, No. 115860.
(37) Huang, H.; Zhao, J.; Guo, X.; Deng, B.; Chen, Y.; Huang, X. Study on reducing carbon dioxide and harmful emissions of diesel-ignited natural gas engine. *Chemosphere* **2022**, *306*, No. 135586.
(38) Esonye, C.; Onukwuli, O. D.; Ofoefule, A. U.; Ogah, E. O. Multi-input multi-output (MIMO) ANN and Nelder-Mead's simplex based modeling of engine performance and combustion emission characteristics of biodiesel-diesel blend in CI diesel engine. *Appl. Therm. Eng.* **2019**, *151*, 100−114.
(39) Dey, S.; Reang, N. M.; Das, P. K.; Deb, M. Comparative study using RSM and ANN modelling for performance-emission prediction of CI engine fuelled with bio-diesohol blends: A fuzzy optimization approach. *Fuel* **2021**, *292*, No. 120356.
(40) Baak, M.; Koopman, R.; Snoek, H.; Klous, S. A new correlation coefficient between categorical, ordinal and interval variables with Pearson characteristics. *Comput. Stat. Data an.* **2020**, *152*, No. 107043.
(41) Dey, S.; Reang, N. M.; Majumder, A.; Deb, M.; Das, P. K. A hybrid ANN-Fuzzy approach for optimization of engine operating parameters of a CI engine fueled with diesel-palm biodiesel-ethanol blend. *Energy* **2020**, *202*, No. 117813.
(42) Roy, S.; Banerjee, R.; Bose, P. K. Performance and exhaust emissions prediction of a CRDI assisted single cylinder diesel engine coupled with EGR using artificial neural network. *Appl. Energy* **2014**, *119*, 330−340.
(43) Yin, X.; Li, Z.; Yang, B.; Sun, T.; Wang, Y.; Zeng, K. Experimental study of the combustion characteristics prediction model for a sensorless closed-loop control in a heavy-duty NG engine. *Fuel* **2021**, *300*, No. 120945.
(44) Zhang, Y.; Fu, J.; Shu, J.; Xie, M.; Zhou, F.; Liu, J.; Zeng, D. A numerical investigation of the effect of natural gas substitution ratio (NGSR) on the in-cylinder chemical reaction and emissions formation process in natural gas (NG)-diesel dual fuel engine. *J. Taiwan Inst. Chem. E.* **2019**, *105*, 85−95.
(45) Vadlamudi, S.; Gugulothu, S. K.; Panda, J. K.; Deepanraj, B.; Kumar, P. R. V. Paradigm analysis of performance and exhaust emissions in CRDI engine powered with hydrogen and Hydrogen/CNG fuels: A green fuel approach under different injection strategies. *Int. J. Hydrogen Energy* **2022**.
(46) Fırat, M.; Okcu, M.; Altun, Ş.; Varol, Y. Numerical investigation of natural gas (NG) as low reactivity fuel in a reactivity controlled compression ignition (RCCI) engine model. *Fuel* **2023**, *343*, No. 127949.
(47) Mehra, R. K.; Duan, H.; Luo, S.; Rao, A.; Ma, F. Experimental and artificial neural network (ANN) study of hydrogen enriched com-

https://doi.org/10.1021/acsomega.3c01636
ACS Omega 2023, 8, 18212−18224

pressed natural gas (HCNG) engine under various ignition timings and excess air ratios. *Appl. Energy* **2018**, *228*, 736−754.
(48) Uslu, S.; Celik, M. B. Prediction of engine emissions and performance with artificial neural networks in a single cylinder diesel engine using diethyl ether. *Engineering Science and Technology, an International Journal* **2018**, *21*, 1194−1201.
(49) Atelge, M. R. Investigation of a ternary blend of diesel/ethanol/n-butanol with binary nano additives on combustion and emission: A modeling and optimization approach with artificial neural networks. *Fuel Process. Technol.* **2022**, *229*, No. 107155.
(50) Ma, Q.; Zhang, Q.; Chen, Z.; Liang, J. The energy analysis and performance of heavy-duty diesel engine with n-butanol addition and different coolant temperature. *Fuel* **2022**, *316*, No. 123323.

https://doi.org/10.1021/acsomega.3c01636
ACS Omega 2023, 8, 18212−18224